Open sea OWC motions and mooring loads monitoring at BiMEP

S.D. Weller[#1], D. Parish[#2], T. Gordelier[#3], B. de Miguel Para[*4], E.A. Garcia[*5], P. Goodwin[†6], D. Tornroos[†7] and L. Johanning[#8]

[#]*Renewable Energy, University of Exeter*
Penryn Campus, Treliever Road, Penryn, Cornwall, TR10 9EZ United Kingdom
[1]s.weller@exeter.ac.uk, [2]d.n.parish@exeter.ac.uk, [3]t.j.gordelier@exeter.ac.uk, [8]l.johanning@exeter.ac.uk

**Oceantec Energías Marinas, SL, Astondo Bidea – Edificio KABI 612,*
Parque Tecnológico de Bizkaia, 48160 Derio – Bizkaia, Spain
[4]bdemiguel@oceantecenergy.com, [5]ealdaiturriaga@oceantecenergy.com

[†] *Global Maritime Consultancy Ltd., Saddlers' House,*
First Floor, 26 Finsbury Square, London EC2A 1DS, United Kingdom
[6]paul.goodwin@globalmaritime.com, [7]daniel.tornroos@globalmaritime.com

***Abstract* - Despite the large number of wave energy converter concepts proposed over the past three decades, only a few field measurement datasets are available in the public domain. The sparse nature of device performance and reliability data coupled with a general lack of design convergence means that technological and economic progress within the sector is fragmented. Fundamental to ensuring device efficiency and survivability is the acquisition of long-term, open sea, device and mooring system response data, combined with comprehensive numerical modelling. With mooring systems representing approximately 10% of marine renewable energy device CAPEX, the evolution of shared mooring systems and the use of novel materials with load reduction capabilities represent clear strategies to achieve more favourable project finances.**

This paper will report on design of the mooring load monitoring system as well as preliminary analysis of several load cases identified from field data recorded during the winter of the first deployment. Comparisons are made to numerical simulations of the device and mooring system subjected to representative environmental conditions. The measured mooring line tensions also provide operational design criteria (i.e. load capacity and durability requirements) for two elastomeric tethers which will replace the polyester ropes currently used in the seaward catenary lines.

***Keywords* - Oscillating Water Column; Karratu Shared Mooring System; Field Measurements; Numerical Simulations; BiMEP**

I. Introduction

Perceived regulatory, market and technological risks are perhaps the greatest impediment to progress within the marine renewable energy (MRE) sector and have a direct influence on project finances [1]. Risks can be mitigated by knowledge and data sharing; providing device developers with insight to avoid repetition of project failures and reducing uncertainties for project financiers and regulators. Ideally such cooperation would be commonplace, however a general lack of wave energy design convergence coupled with concerns of commercial competitiveness and intellectual property has hampered this process and only a handful of grid-connected devices have so far been deployed [2]. Encouragingly there have been several relevant initiatives to encourage knowledge and data sharing, such as for wind turbine and offshore equipment reliability (e.g. [3, 4]) as well as MRE device performance estimation (e.g. [5]). Adoption of these measures will also enable offshore standards to be developed that are relevant to the MRE sector and perhaps ultimately lead to standardisation.

The Horizon 2020-funded Open Sea Operating Experience to Reduce Wave Energy Cost (OPERA) project aims to contribute to the knowledge base by providing operational experience and field data from two wave energy installations; i) a floating oscillating water column (OWC) moored at the BiMEP site in the Bay of Biscay and ii) a shore-based OWC installed at the Mutriku plant. The project comprises several key innovations including:

- A novel bi-radial turbine and advanced control algorithms
- Shared mooring infrastructure
- An elastomeric mooring tether
- A floating OWC device

On 16th November 2016 commissioning of the Marmok-A-5 OWC device was completed at the BiMEP site by Oceantec Energias Marinas supported by the Basque government energy agency (EVE). This milestone signals the start of the first testing campaign which will serve as a benchmark for two years of open-sea operational data collection as part of the OPERA project.

This paper focuses on preliminary analysis of data captured during the first few months of the MARMOK-A5 device offshore deployment. OWC devices have received considerable attention over the past three decades with applications ranging

from navigation or sensor equipment [6] to larger scale systems [7]. Spar-type devices are an attractive option because they are axisymmetric (and hence do not need to weathervane if the wave direction varies) and the hull structure is based on proven offshore technology. With mooring systems representing a significant portion of MRE project costs [8], the use of novel materials with load reduction capabilities [9, 10] and shared mooring systems [11] have been identified as potential ways of reducing project costs.

The deployed system is outlined in Section II with details provided on the device, mooring system and load measurement equipment. In Section III the results from initial dynamic simulations are presented and compared to field data measured over the first few months of device operation at BiMEP. Section IV includes a discussion of the results and outlines planned future work.

II. Deployed System

A. MARMOK-A5 and Karratu mooring system

The MARMOK-A5 OWC, developed by Oceantec Energias Marinas, comprises a 5m diameter (max) and 41.8m long and 162.2t hollow spar buoy, which for the OPERA project, is deployed in approximately 85m water depth at the BiMEP site (Table 1 and Fig 1).

Fig 1: The MARMOK-A-5 device deployed at BiMEP. One of the pennant buoys supporting a corner node is visible on the right hand side of the photo.

TABLE I
Principal Marmok A-5 parameters

Mass (t)	Total volume (m^3)	Diameter (m)	
		Min	Max
162.19	275.99	2.85	5.0

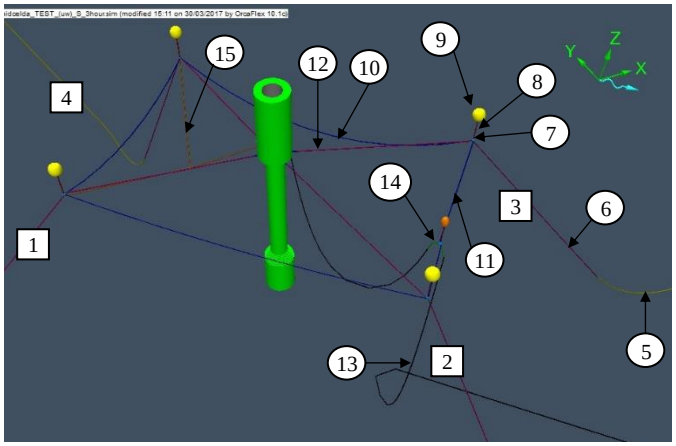

Fig 2: Orcaflex representation of the MARMOK-A-5 device and Karratu mooring system. For clarity, full component details are provided for Mooring Limb 3 only but each mooring limb utilises equivalent components. The predominant wave direction relative to the device is shown in the top right hand corner of this figure.

TABLE II
MOORING LIMB DETAILS[1]

#	Item	Diameter	Max length	Dry weight
1	Mooring Limb 1	*Mooring assembly: Detailed example Item 3*		
2	Mooring Limb 2	*Mooring assembly: Detailed example Item 3*		
3	Mooring Limb 3	*Mooring assembly: Comprising components 5, 6, 7, 8, 9 and 12.*		
4	Mooring Limb 4	*Mooring assembly: Detailed example Item 3*		
5	Catenary chain (studlink)	1.0	1.0	1.0
6	Catenary rope (polyester)	1.82	0.157	0.094
7	Connecting Node	-	-	1.0
8	Buoy chain (studless)	0.73	0.009	0.494
9	Pennant buoy	36.36	0.004	8.182
10	Cell line C (wire rope)	0.36	0.116	0.023
11	Cell line B (wire rope)	0.36	0.072	0.023
12	Connex rope (polyester)	1.82	0.06	0.094
13	Umbilical	1.14	~	0.15
14	Bend restrictor	-	-	14.478
15	Load shackle cable system	*See Section IIB*		

[1] All values are non-dimensionalised by Item 5 values with the exception of dry unit weights for Items 9 and 14 which are non-dimensionalised by Item 7.

The mooring system is one square cell of the shared 'Karratu' system proposed in [11]. The motivation for using this design is to reduce the number of mooring and anchoring components, thereby reducing costs and increasing the reliability for arrays of MRE devices. Referring to Fig 2 and Table II and starting at the anchors, there are four Catenary limbs comprising studlink chain and polyester rope (5 and 6). The limbs are connected to nodes (7) at the corners of the Karratu cell and each node is supported by a chain (8) and pennant buoy (9). Joining the nodes are wire ropes (10-11) which form the sides of the cell. The MARMOK A-5 device is connected to four polyester Connex lines (12) which are also joined to the corner nodes. The power/signal umbilical (13) is supported on the leeward side of the mooring system by a bend restrictor (14) which is connected to Cell line B (11). This connection point is supported by a studless chain and pennant buoy (not labelled in Fig 2). Measurements from the seaward load shackles are transferred to MARMOK via signal cables supported by a load shackle cable support system (15) which will be discussed in the next section.

B. Load shackle cable system (LSCS)

The Karratu mooring system is orientated to the predominant wave direction (311°) based on long-term wave monitoring at BiMEP [12]. This wave direction is highlighted by the blue arrow in Fig 2. Numerical modelling (detailed in Section III) established Mooring Limbs 1 and 4 as carrying the peak mooring loads. The condition monitoring system is therefore designed around these two limbs, capturing the loads on both the Catenary rope (connecting the node to the Catenary chain and then the anchor) and the Connex line (connecting the node to the OWC hull).

Load shackles are selected as the preferred load monitoring hardware to facilitate simple substitution of components and to maintain the existing network mooring system architecture. 55t standard bow shackles are specified with the safety bolts replaced with bespoke load pins manufactured from 17-4PH H1075 stainless steel to match the specific dimensions of each shackle. Utilising this steel for the pins maintains the specified safety factor of 6, equating to a minimum breaking load (MBL) of 330t. A strain relief bracket is mounted on the load pin head to provide strain relief for the cable connector, and a signal amplifier is installed within each load pin head (Fig 3). Each load shackle is connected to the OWC hull Junction Box via a four core signal cable. Three of these cores are used for +24V DC, 0V DC and 4-20mA (measured with respect to 0V). The load shackles are calibrated such that:

$$\text{4-20mA output} = 0 - 813\text{kN}$$

Fig 3: A 55t load shackle with bespoke pin fitted with strain relief bracket and signal amplifier.

The ideal location for load monitoring of Connex lines 1 and 4 is at the OWC hull; however, due to conflicts in component compatibility at the hull, it was necessary to locate the load shackles at the nodes. The load monitoring for Catenary ropes 1 and 4 is also located at the nodes. Fig 4 details the configuration of the load shackles in relation to the node design.

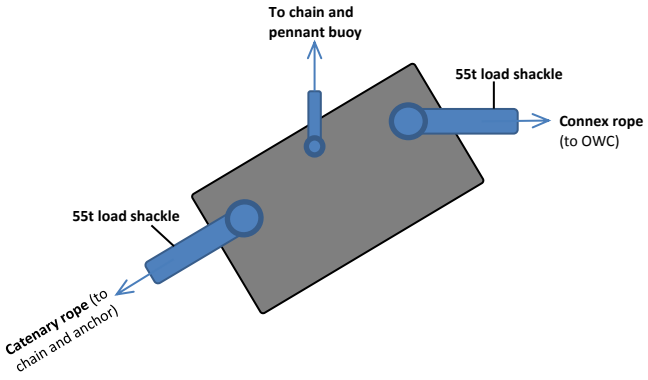

Fig 4: Orientated configuration of load monitoring shackles and node. Identical configuration used for Nodes 1 and 4.

Due to the highly dynamic nature of both the OWC and the network mooring system, routing the load shackle signal cables back to the OWC for connection into the OWC hull Junction Box is a significant design challenge. Various cabling routes were considered, utilising a range of cable types. Numerical modelling was used to assess potential peak loads, as well as line and hull clashes.

Referring to Fig 5 the optimum solution identified utilises a load shackle cable support (LSCS) system to support the load shackle cables. The signal cables run along 14mm wire rope from Node 1 and Node 4 to meet at a central weight (the Tri-Weight) hung between the nodes and the OWC hull. From this central weight, all four load shackle signal cables are routed back to the OWC hull along another section of 14mm wire rope. This system can be seen in Fig 2, Item 15. Utilising the wire rope provides stiffness and a uniformly distributed mass to bias the bundle and lines away from the hull of MARMOK and Connex lines without creating excessive loads in the line. Numerical modelling has demonstrated that this configuration maintains the tension load on the OWC hull well below the 1t specified limit, whilst eliminating line clashing and minimising

clashing with the OWC hull in all but 1 in 100 year storm conditions.

Spiral binding is installed around each load shackle cable to prevent wear with the wire rope and a further layer of spiral binding is installed around the load shackle cable and wire rope bundles to secure the components together. Cable ties are utilised to clamp the bundle together at 0.5m intervals and more spiral binding and marine sealant adhesive are used to mould additional support around the critical junctions such as the nodes and at the Tri-Weight junctions.

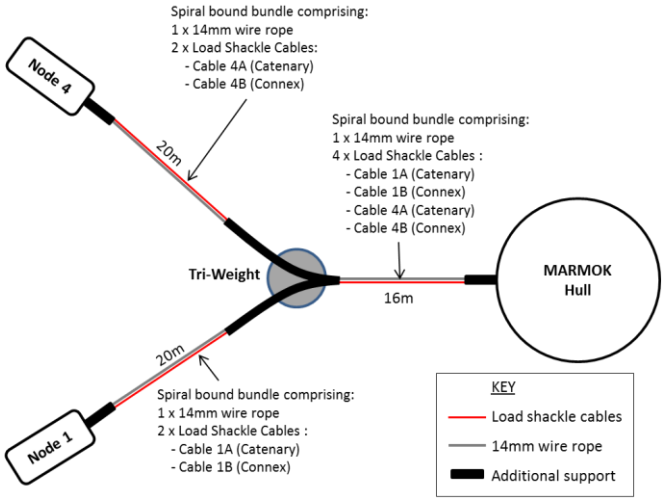

Fig 5: Load shackle cable support system schematic. For clarity the mooring system architecture, Nodes 2 and 3, and the connecting hardware are not included. Not to scale.

The Tri-Weight to OWC section of wire rope is terminated at an eye installed at the bottom of the OWC hull, and the load shackle cables are fed up through two acetal plastic J-tubes attached to the OWC hull. The cables are then terminated in a Junction Box, located at the top of the OWC hull. From the Junction Box a single 14 core DAQ cable is routed around the outside of the hull and into the central DAQ system, which is accessible from the leeward side of the hull.

III. Preliminary Numerical Simulations and Comparison to Field Data

Description of environmental data gathered

Environmental data has been gathered from:

- Wave - TRIAXYS Directional Wave Buoy, moored in 85m water-depth, located within the mooring spread of MARMOK. The summary parameters used in this study include H_s, T_p, T_z and direction.
- Wind – interpolated from a CNT model point (2.88deg W, 43.46deg N) close to MARMOK nominal position. Values provided by the AEMET (Spanish Meteorological Agency).
- Current – from an IBI model point 3159035 (2.88deg W, 43.46deg N) provided by the Copernicus IBI-MFC Ocean Analysis and Forecasting System.

Description of measured data (6 degree of freedom DoF, tension)

A motion response unit (IMU) and integrated GPS system located on the MARMOK records surge, sway, heave, roll, pitch and yaw. The GPS antenna and IMU are at known locations on the MARMOK device.

Additionally a load shackle has been in operation on Mooring Limb 1 of the mooring system, at the connection between the upper-end of the polyester section and corner node.

Description of numerical model

A numerical model of the MARMOK device and mooring system has been set-up in Orcaflex software. The model attempts to replicate the actual moored device and mooring system.

Environmental parameters

From review of the field measured environmental data, nine, 20-minute samples of environment have been selected that represent different types of sea-state:

A. Low sea-state (Case 1 to 3)
B. Moderate sea-state (Case 4 to 6)
C. High energy sea-state (case 7 to 9)

The environmental conditions are summarised in Table III.

TABLE III
Environmental Conditions Considered in this Study

Case	Wave				Wind		Current	
	H_s (m)	T_p (s)	T_z (s)	Dir (°)	V_w (m/s)	Dir (°)	V_c (m/s)	Dir (°)
1	1.19	9.1	5.9	293	7.25	196	0.29	261
2	1.15	9.5	6.3	298	7.25	196	0.29	261
3	1.11	9.5	6.3	297	6.38	197	0.29	263
4	2.61	14.3	10.4	306	6.56	179	0.2	242
5	2.55	13.3	9.6	305	6.56	179	0.2	242
6	2.12	14.3	9.2	304	6.56	179	0.2	242
7	4.17	15.4	8.2	304	8.23	280	0.18	276
8	4.38	15.4	9.3	305	8.23	280	0.18	276
9	4.83	13.3	9.4	304	8.23	280	0.18	276

The actual spectral distribution of the measured wave had not been retained from the TRIAXYS measurement buoy. Based on prior analysis carried out at BiMEP, a JONSWAP spectrum has been assumed for the analysis [12]. The peakedness parameter has been chosen to attempt to match T_z for a given T_p, see Table IV. No directional wave spreading has been applied.

TABLE IV
WAVE PARAMETERS APPLIED

Case	Wave	
	Peakedness parameter applied	T_z attained (s)
1	3.31	7.08
2	1.0	6.47
3	1.0	6.75
4	1.4	10.39
5	1.4	9.67
6	1.0	10.16
7	1.0	10.94
8	1.0	10.94
9	1.0	9.45

Heave Motion

The mean, standard deviation and min-max range of the heave time traces are presented in Table V. A percentage difference has been evaluated for the standard deviation and range parameters between measured and analysis values. The heave from the analysis tends to be smaller than the measured heave. In general, the % difference for heave standard deviation and range increases as the H_s increases. The difference between the measured and analysed results might be attributed to:

- difference in the wave energy distribution between measured and numerical model, consequently affecting the heave forcing
- the amount of heave damping applied in the model
- effect of the restriction in air flow out of the chamber on the MARMOK device due to the chamber geometry and air turbine

TABLE V
HEAVE MOTION AT CENTRE OF GRAVITY (UNITS: M)

Case	Mean		Std Dev			Range		
	Measured	Analysis	Measured	Analysis	% Diff	Measured	Analysis	% Diff
1	0.00	0.01	0.55	0.52	-5%	3.23	3.25	1%
2	0.00	0.01	0.50	0.56	12%	3.36	3.39	1%
3	0.00	0.01	0.50	0.52	4%	3.36	2.82	-16%
4	0.01	0.03	0.96	0.88	-8%	5.82	5.69	-2%
5	0.00	0.03	0.91	0.82	-10%	6.49	4.97	-23%
6	0.00	0.02	0.84	0.72	-14%	5.43	4.64	-15%
7	0.00	0.07	1.67	1.20	-28%	10.11	7.18	-29%
8	0.00	0.08	1.68	1.26	-25%	10.18	7.45	-27%
9	0.00	0.10	1.75	1.49	-15%	10.74	9.96	-7%

Heave Motion Spectra

Heave motion spectra are presented in Fig 6 to Fig 8. There is relatively good comparison between measured and analysis based spectra. Both the numerical model and measured heave present a peak in the response that is associated with the peak period of the sea-state. However, the numerical model also presents a peak response at 1.3rad/sec (0.21 Hz). This is attributable to the heave natural period in the numerical model. Some sources of the difference have been indicated in the previous paragraph. The heave spectra also serve to indicate the nature of this difference, particularly the frequency distribution of the heave motion energy. It is necessary to understand the root cause of these differences, in order to make adjustments to the model and so improve this comparison.

Mooring Line Tension

The mean, standard deviation and min-max range of the tension time trace are presented in Table VI. A percentage difference has been evaluated for these parameters.

The difference in mean tension predicted from the numerical model compared with the measured model is small for the moderate sea-states (1%), whereas it is +20% for the Low sea-states and -20% for the High sea-states. This implies that there is underlying cause of difference from wind, wave and current mean load components. As well as the loading model, the direction of the environment will impact on the steady loads observed by the mooring lines.

The difference in standard deviation of tension varies by ±30%. The wave energy is likely to be the predominant source of MARMOK response and mooring tension oscillations. As discussed previously the distribution of this wave energy is not accurately known. This may be a contributory factor to the difference in standard deviation and Min-Max range of tensions between measured and numerical analysis.

TABLE VI
TENSION AT NODE END OF CATENARY (LIMB 1) (UNITES: KN)

Case	Mean			Std Dev			Min-Max Range		
	Measured	Analysis	% Diff	Measured	Analysis	% Diff	Measured	Analysis	% Diff
1	24.5	29.6	21%	1.61	1.68	4%	12.2	12.6	3%
2	24.3	29.9	23%	1.59	2.13	34%	11.9	17.0	43%
3	24.3	29.6	22%	1.59	1.73	9%	11.9	15.4	29%
4	27.5	27.3	1%	1.96	2.27	16%	16.7	20.1	20%
5	27.2	27.5	1%	1.91	2.28	19%	14.9	20.8	40%
6	27.0	27.2	1%	1.88	1.69	10%	15.3	14.2	7%
7	37.2	29.5	21%	6.70	4.92	27%	54.9	51.2	7%
8	36.3	29.6	18%	6.24	5.40	13%	53.6	58.0	8%
9	37.5	31.9	15%	7.23	8.38	16%	70.9	89.3	26%

IV. CONCLUSIONS

It has been the purpose of this paper to report on initial comparisons between measured field data and numerical simulation results conducted as part of the OPERA project. A fundamental aim of the project is the dissemination of knowledge and data in order to de-risk innovations and in turn reduce both project costs and risks for the benefit of the sector. An overview of the MARMOK-A5 device and Karratu mooring system, including the equipment used to monitor mooring line tensions and device motions has been provided. The practicalities of providing a data link between the corner nodes of the Karratu mooring system and MARMOK-A5 device have been addressed.

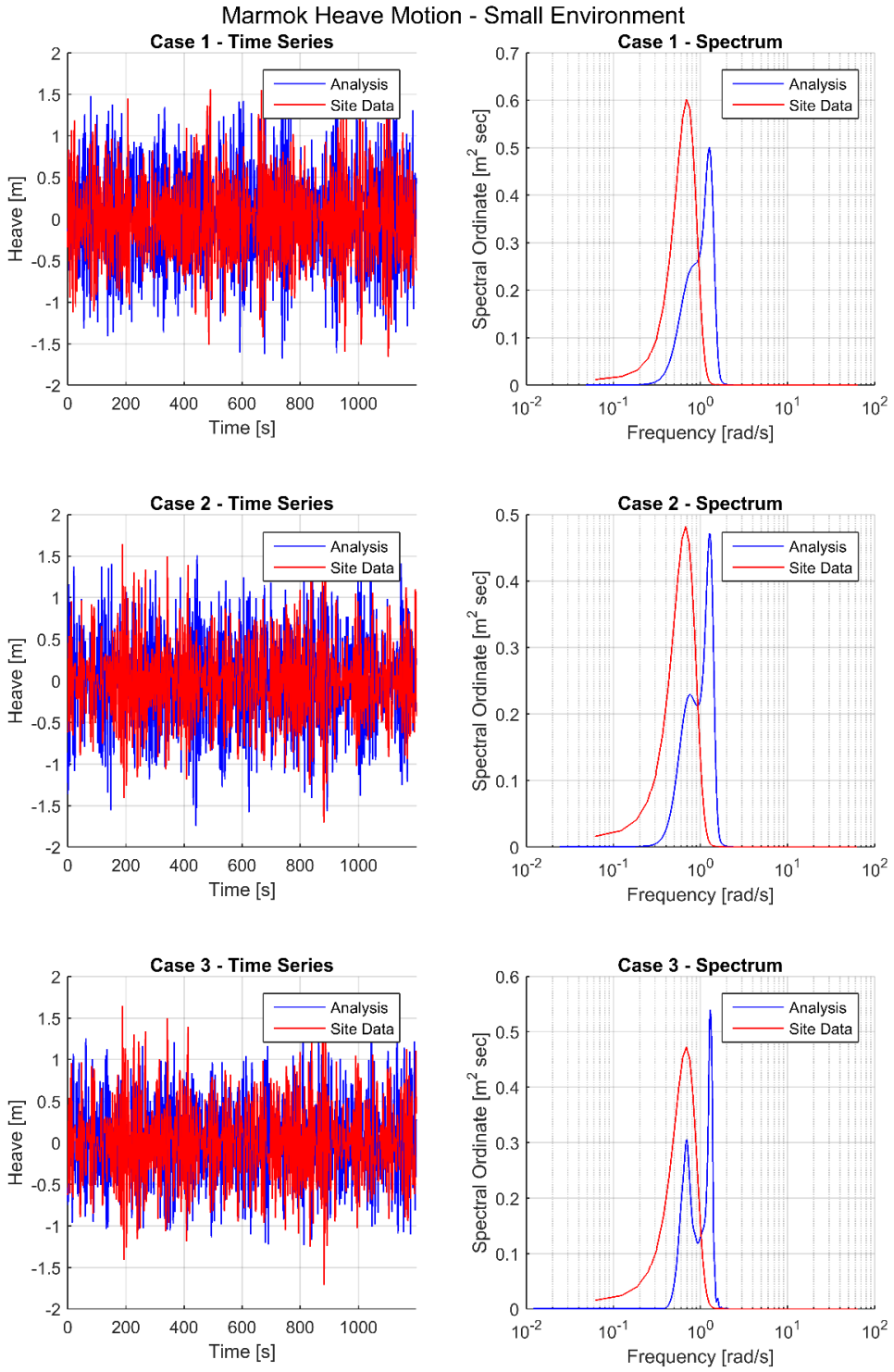

Fig 6: Heave motion time trace and spectral density at Centre of Gravity – Low Sea-state

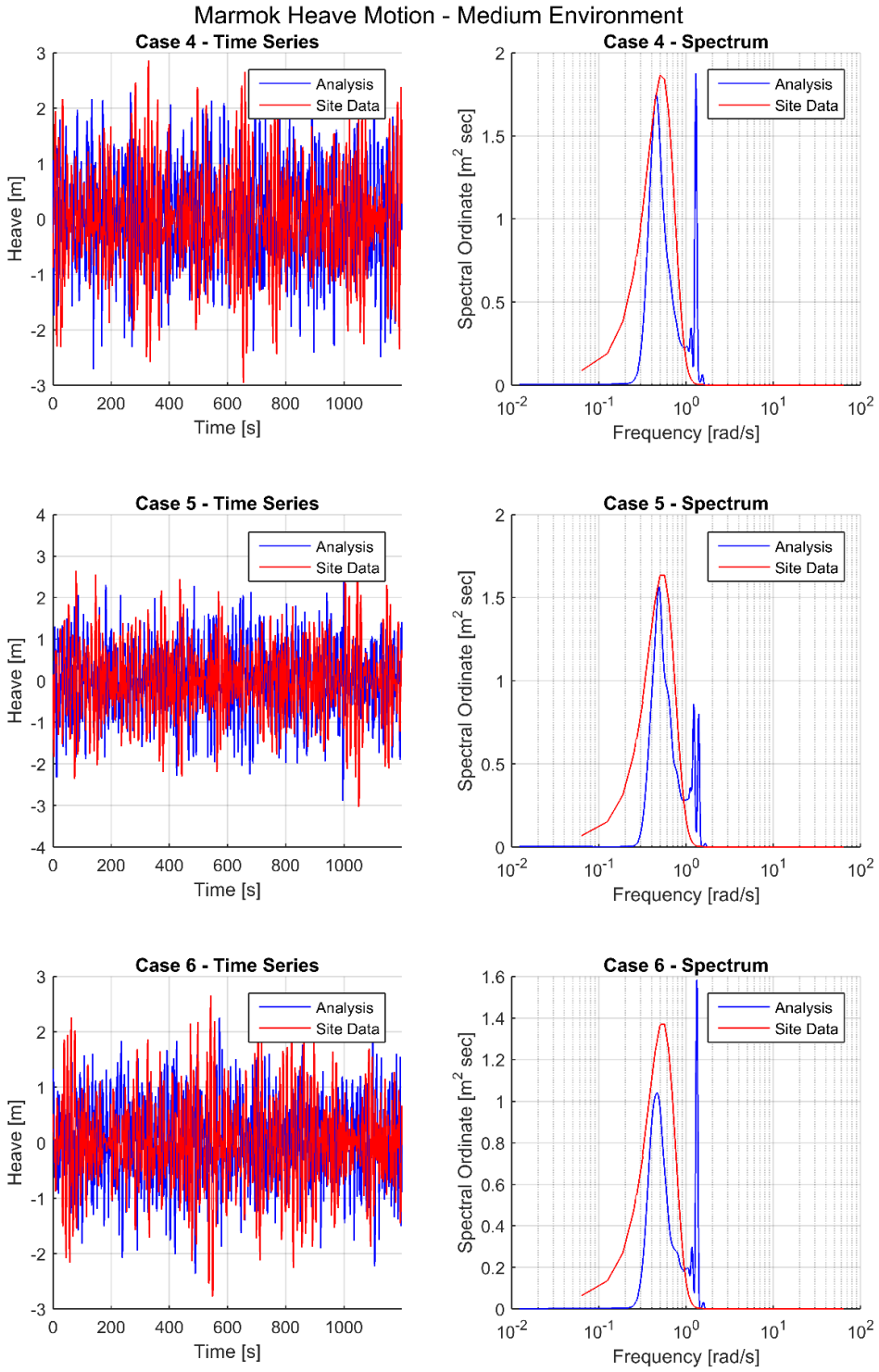

Fig 7: Heave motion time trace and spectral density at Centre of Gravity – Medium Sea-state

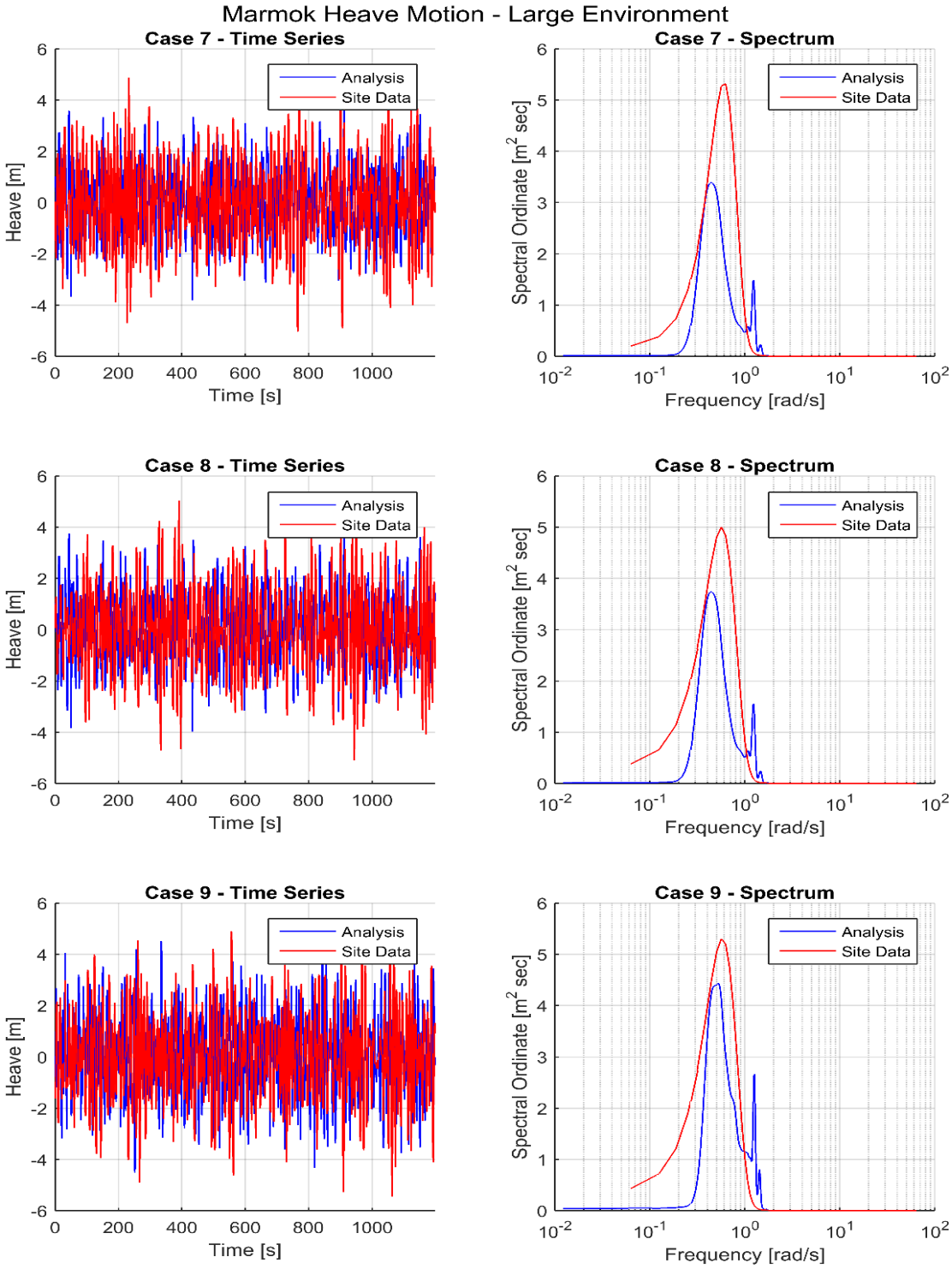

Fig 8: Heave motion time trace and spectral density at Centre of Gravity – Large Sea-state

The statistics calculated from field data and simulation results indicate that use of summary wave buoy data, in addition to modelled (localised) wind and current conditions can provide an adequate preliminary representation of the mean, standard deviation of heave motions and line tensions. Comparison of the spectral content of measured and simulation spectra has demonstrated a favourable level of agreement in the moderate and large sea-states, indicating that the heave natural period of the model is close to that associated with the actual device and mooring system. Tension ranges were less well represented by the numerical model and this discrepancy warrants further investigation.

It is acknowledged that there are several shortcomings in the current numerical model. These include the lack of power take-off system representation and the fact that second-order wave effects are not accounted for 6 DoF buoys in the current version of Orcaflex. However, the work reported here represents the start of numerical model development of the MARMOK-A5 device and Karratu mooring system. Refinement of the model will be guided by a detailed validation programme which will utilise live field measurements. Following validation of the model during the first and second deployments an assessment will be made into the dynamics of a larger Karratu mooring system comprising multiple devices (and hence several mooring cells). The response of an array of devices is likely to differ from the single device and cell featured in this paper, with the behaviour of individual devices dependent on the loads transferred through the shared mooring system. In addition, if the devices are positioned in close proximity, hydrodynamic interactions occurring between the devices [13] may also influence device response, mooring system loads and device power generation.

V. Future work

The objectives of future work include:

- Utilisation of measured surface elevations allowing time domain analysis to be conducted. This will build upon the simulations reported in this paper which were based on summary wave buoy conditions.
- Development of a higher resolution model which can account for the power take-off system.
- Representation of Deployment 2 which features two elastomeric tethers which will replace polyester ropes currently used in the seaward catenary lines.
- Assessment of the shared Karratu mooring system in the presence of two or more devices.

Acknowledgment

The research leading to this paper is part of the OPERA (Open Sea Operating Experience to Reduce Wave Energy Cost) project which is funded from the European Union's Horizon 2020 research and innovation programme under grant agreement No 654.444.

References

[1] Ocean Energy Forum, "Ocean Energy Strategic Roadmap. Building Ocean Energy for Europe," 2016.

[2] Energy Research Knowledge Centre, "Overcoming Research Challenges for Ocean Renewable Energy," 2013.

[3] S. S. Sheng, "Report on Wind Turbine Subsystem Reliability ─ A Survey of Various Databases," 2013.

[4] OREDA, "OREDA Handbook 2015, 6th edition – Volume I and II," 2015.

[5] DHI , "SI Ocean: Tidal & Wave Energy," 2017. [Online]. Available: http://si-ocean.dhigroup.com/map. [Accessed 15 3 2017].

[6] J. C. C. Henriques, J. C. C. Portillo, L. M. C. Gato, R. P. F. Gomes, D. N. Ferreira and A. F. O. Falcão, "Design of oscillating-water-column wave energy converters with an application to self-powered sensor buoys," *Energy*, vol. 112, p. 852–867, 2016.

[7] A. F. de O. Falcão , "Wave energy utilization: A review of the technologies," *Renewable and Sustainable Energy Reviews*, vol. 14, no. 3, p. 899–918, 2010.

[8] Carbon Trust and Black & Veatch , "Accelerating marine energy. The potential for cost reduction – insights from the Carbon Trust Marine Energy Accelerator.," 2011.

[9] S. D. Weller, L. Johanning, P. Davies and S. J. Banfield, "Synthetic mooring ropes for marine renewable energy applications," *Renewable Energy*, vol. 83, pp. 1268-1278, 2015.

[10] D. Parish, M. Herduin, T. Gordelier, P. R. Thies and L. Johanning, "Reducing Peak & Fatigue Mooring Loads: A Validation study for Elastomeric Moorings.," in *Proc. of the 12th European Wave and Tidal Energy Conference*, Cork, Ireland, 2017.

[11] P. Ricci, A. Rico, P. Ruiz-Minguela, F. Boscolo and J. L. Villate, "Design, Modelling and Analysis of an Integrated Mooring System for Wave Energy Arrays," in *Proc. of the 4th International Conference on Ocean Energy*, Dublin, Ireland, 2012.

[12] BiMEP and IH Cantabria, "Metocean Analysis of BiMEP for Offshore Design," 2017.

[13] S. D. Weller, T. J. Stallard and P. K. Stansby, "Experimental measurements of irregular wave interaction factors in closely spaced arrays," *IET Renewable Power Generation*, vol. 4, no. 6, pp. 628-637, 2010.